LETTER

Tuning of thermoelectric properties with changing Se content in Sb_2Te_3

To cite this article: D. Das *et al* 2016 *EPL* **113** 47004

A Letters Journal Exploring the Frontiers of Physics

February 2016

EPL, **113** (2016) 47004 www.epljournal.org
doi: 10.1209/0295-5075/113/47004

Tuning of thermoelectric properties with changing Se content in Sb_2Te_3

D. Das[1], K. Malik[2], A. K. Deb[3], V. A. Kulbachinskii[4], V. G. Kytin[4], S. Chatterjee[5], D. Das[5], S. Dhara[6], S. Bandyopadhyay[1,7] and A. Banerjee[1,7(a)]

[1] *Department of Physics, University of Calcutta - 92 A P C Road, Kolkata-700009, India*
[2] *Department of Physics, Vidyasagar Evening College - 39 Sankar Ghosh Lane, Kolkata-700006, India*
[3] *Department of Physics, Raiganj University - Uttar Dinajpur 733134, India*
[4] *Department of Low Temperature Physics and Superconductivity, Physics Faculty, M.V. Lomonosov Moscow State University - 119991, Moscow, Russia*
[5] *UGC-DAE Consortium for Scientific Research, Kolkata Centre, Sector III, LB-8 - Salt Lake, Kolkata-700098, India*
[6] *Surface and Nanoscience Division, Indira Gandhi Centre for Atomic Research - Kalpakkam 603102, India*
[7] *Center for Research in Nanoscience and Nanotechnology, University of Calcutta, JD-2, Sector-III Salt Lake, Kolkata-700098, India*

received 16 December 2015; accepted in final form 24 February 2016
published online 9 March 2016

PACS 72.20.Pa – Thermoelectric and thermomagnetic effects
PACS 72.20.-i – Conductivity phenomena in semiconductors and insulators
PACS 61.05.cp – X-ray diffraction

Abstract – Polycrystalline $Sb_2Te_{3-x}Se_x$ ($0.0 \leq x \leq 1.0$) samples were synthesized by the solid-state reaction method. The structural analysis showed that up to the maximal concentration of Se, the samples possess rhombohedral crystal symmetry (space group $R\bar{3}m$). The increase of Se content increases the resistivity of the samples. The variation of phonon frequencies, observed from the Raman spectroscopic study, depicts an anomalous behaviour around $x = 0.2$. The sample $Sb_2Te_{2.8}Se_{0.2}$ also shows maximum Seebeck coefficient, carrier concentration and thermoelectric power factor. The nature of the scattering mechanism controlling the thermopower data has been explored. The thermoelectric properties of the synthesized materials have been analyzed theoretically in the frame of the Boltzmann equation approach.

Introduction. – The thermoelectric (TE) effect refers to the phenomenon of direct conversion of heat to electric voltage and vice versa [1,2]. The efficiency of a TE material can be quantitatively expressed by the dimensionless term *figure of merit*, $ZT = \frac{S^2}{\rho\kappa}T$, where S, ρ and κ, are, respectively, the Seebeck coefficient, the electrical resistivity and the thermal conductivity of the TE material and T is the absolute temperature. By maximizing the power factor ($PF = S^2/\rho$) and/or lowering the thermal conductivity, ZT can be improved [3,4]. Antimony telluride (Sb_2Te_3) is a well-known p-type TE material for near room temperature applications [5–8]. The incorporation of Se atoms into a Sb_2Te_3 lattice modifies the nature of defect states, which, in principle, should lead to interesting changes in its TE properties. Efforts were thus devoted to study the effect of Se doping on the structural [9], transport [10], electronic band structure [5] and TE [11] properties of Sb_2Te_3 alloys. Some anomalous behaviour was reported in the range $x = 0.0$–1.0 for the $Sb_2Te_{3-x}Se_x$ system, which needs further attention. On the contrary, Bi_2Te_3-based chalcogenides, *viz.*, $Bi_2Te_{3-x}Se_x$, including the most compensated compound Bi_2Te_2Se, are well explored [12,13].

Here we investigate different compositions of the $Sb_2Te_{3-x}Se_x$ ($0.0 \leq x \leq 0.1$) alloy. Room temperature powder X-ray diffraction (XRD) and thermal variation of resistivity, $\rho(T)$ data show a systematic variation with the Se content. However, the S, PF, Hall carrier concentration of the charge carriers (n_H), and the Raman spectroscopic study show some anomalous behaviour around $x = 0.2$. In this report, an attempt has been made to elucidate the origin of this anomalous behaviour. In addition, the $S(T)$, $\rho(T)$, $n_H(T)$ and PF data have also been theoretically simulated. The evaluation of the band energy spectrum with the Se content is predicted.

(a) E-mail: arbphy@caluniv.ac.in (corresponding author)

Table 1: Rietveld refinement parameters, *viz.*, lattice parameters, unit cell volume, position coordinates, site occupancy, Debye-Waller factor ($B_{\rm iso}$), reliability parameters ($R_{\rm w}$ (%), $R_{\rm b}$ (%), and $R_{\rm exp}$ (%)), and goodness of fit (Gof or χ^2) value, as obtained using MAUD software for the samples $Sb_2Te_{3-x}Se_x$ (x = 0.0, 0.2, 0.6, and 1.0). The corresponding values of the estimated errors are also provided.

Phase	Sb_2Te_3 [$R\bar{3}m$]	$Sb_2Te_{2.8}Se_{0.2}$ [$R\bar{3}m$]	$Sb_2Te_{2.4}Se_{0.6}$ [$R\bar{3}m$]	Sb_2Te_2Se [$R\bar{3}m$]
Cell (Å)	a: 4.2558 (4.3×10^{-5}) c: 30.3629 (7.4×10^{-4})	a: 4.2403 (1.2×10^{-4}) c: 30.3134 (1.1×10^{-3})	a: 4.2096 (1.1×10^{-4}) c: 30.1278 (1.1×10^{-3})	a: 4.1781 (1.6×10^{-4}) c: 29.8964 (1.6×10^{-3})
Cell volume	476.25	472.02	462.36	451.97
$Sb_x/Sb_y/Sb_z$	0.0 / 0.0/ 0.3994 (4.1×10^{-5})	0.0 / 0.0/ 0.6027 (6.2×10^{-5})	0.0 / 0.0/ 0.3962 (4.3×10^{-5})	0.0 / 0.0/ 0.3943 (4.7×10^{-5})
$Te1_x/Te1_y/Te1_z$	0.0 / 0.0/ 0.7874(2.4×10^{-5})	0.0 / 0.0/ 0.7879(4.0×10^{-5})	0.0 / 0.0/ 0.7867(2.9×10^{-5})	0.0 / 0.0/ 0.7860(3.5×10^{-5})
$Se1_x/Se1_y/Se1_z$	–	Te2/ Se1: 0.0/ 0.0/ 0.0	Te2/ Se1: 0.0/ 0.0/ 0.0	0.0/ 0.0/ 0.0
$B_{\rm isoSb/Te1/Se1}$	Sb: 2.619 (0.026) Te1: 1.522 (0.032) Te2: 0.147 (0.029)	Sb: 1.1917 (0.021) Te1: 1. 1917 (equal), Te2/Se1: 1.1917 (equal)	Sb: 1.8722 (0.020) Te1: 1.8722 (equal), Te2/Se1: 1.8722 (equal)	Sb: 1.544 (0.024) Te1: 1.544 (equal), Se1: 1.544 (equal)
$R_{\rm w}$ (%)	3.941	5.967	5.171	4.814
$R_{\rm b}$ (%)	3.091	4.617	4.089	3.819
$R_{\rm exp}$ (%)	2.104	4.602	4.115	3.886
Gof or χ^2	1.873	1.296	1.257	1.239

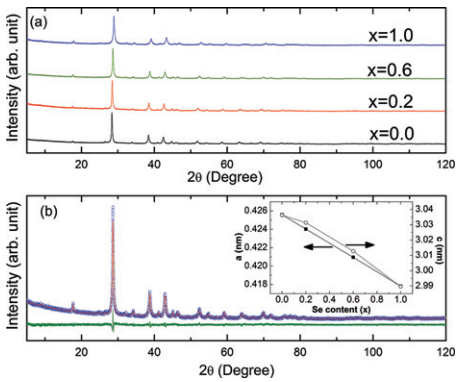

Fig. 1: (Color online) (a) X-ray diffraction patterns of the samples $Sb_2Te_{3-x}Se_x$ (x = 0.0, 0.2, 0.6, and 1.0). (b) X-ray diffraction pattern of the sample $Sb_2Te_{2.8}Se_{0.2}$ after Rietveld refinement. The inset shows the variation of the lattice constants, a and c, with the Se composition for all the samples.

Experimental. – Polycrystalline $Sb_2Te_{3-x}Se_x$ (x = 0.0, 0.2, 0.6, 1.0) samples were synthesized by the solid-state reaction method [6]. The details of the structural characterization, the $\rho(T)$, $S(T)$ measurements and room temperature Raman spectroscopic studies can be found elsewhere [6]. The temperature-dependent Hall coefficient $R_{\rm H}(T)$ measurements were performed by the van der Pauw method on similar bar samples in a closed cycle refrigerator (CCR)-based 15 T magnet supplied by Cryogenic Ltd., UK.

Results and discussion. – Phase purity and structure of the $Sb_2Te_{3-x}Se_x$ ($0.0 \leq x \leq 1.0$) mixed crystals have been identified by XRD and the corresponding spectra are shown in fig. 1(a). We have performed Rietveld refinement (utilizing the *Materials Analysis Using Diffraction* (MAUD) program) using atomic positions and substitutions of all the synthesized $Sb_2Te_{3-x}Se_x$ (x = 0.0, 0.2, 0.6, 1.0) samples. The space group $R\bar{3}m$ and point group D_{3d} were used for the refinement [14–16]. The refinement parameters are provided in table 1. Figure 1(b) shows a typical refinement result for the $Sb_2Te_{2.8}Se_{0.2}$ sample. The variation of the lattice constant with the Se content for the samples are shown in the inset. The linear contraction of the lattice parameters with increased Se concentration closely follows Vegard's law. The atomic radii of Te and Se are 142 pm and 100 pm, respectively [17]. Thus, substitution of Se at the Te position should lead to a decrease in the lattice parameter and hence the cell volume (table 1). According to Vegard's law, the crystallographic parameters of a continuous substitutional solid solution vary linearly with the concentration when the nature of the bonding is similar in the constituent phases. The XRD results thus confirm that synthesized $Sb_2Te_{3-x}Se_x$ alloys are single phase in nature and a complete solid solution has been formed with Se, substituting Te. However, a close observation reveals that the variation of the lattice parameter a with the Se concentration is exactly linear, *i.e.*, strictly following Vegard's law. However, the variation of the lattice parameter c with the Se content shows a little deviation from linearity around $x = 0.2$. This might be related to the anomaly observed in $S(T)$, $R_{\rm H}(T)$ or $n_{\rm H}(T)$ and PF data of the $Sb_2Te_{2.8}Se_{0.2}$ sample discussed later.

Figure 2 shows room temperature Raman spectra (RS) for all the synthesized samples. The Sb_2Te_3 alloy exhibits

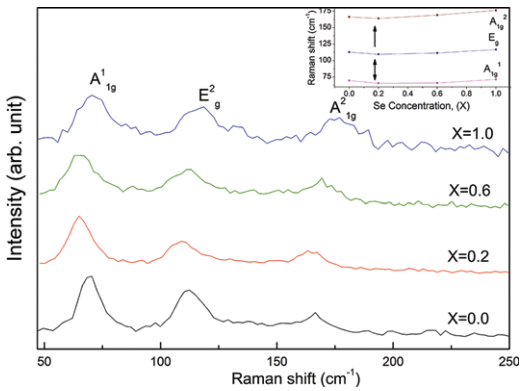

Fig. 2: (Color online) Room temperature Raman spectra of the samples $Sb_2Te_{3-x}Se_x$ ($x = 0.0$, 0.2, 0.6, and 1.0) recorded under excitation at $\lambda = 514.5\,\text{nm}$, indicating the presence of Raman active $A^1_{1g}, E^2_g, A^2_{1g}$ modes. The inset summarizes the observed Raman shifts of different vibrational modes with the Se(x) content for the synthesized $Sb_2Te_{3-x}Se_x$ ($0.0 \le x \le 1.0$) samples.

four Raman active modes: E^1_g ($46\,\text{cm}^{-1}$), A^1_{1g} ($62\,\text{cm}^{-1}$), E^2_g ($113\,\text{cm}^{-1}$) and A^2_{1g} ($166\,\text{cm}^{-1}$) [18–20]. The RS (fig. 2) for Se-doped Sb_2Te_3 alloys depict three peaks at around $69\,\text{cm}^{-1}$, $112\,\text{cm}^{-1}$ and $166.6\,\text{cm}^{-1}$, that can be attributed to Raman active A^1_{1g}, E^2_g, and A^2_{1g} vibrational modes, respectively. The active Raman mode E^1_g (around $46\,\text{cm}^{-1}$) is out of the range measured in this work [6].

Although the Se atom is iso-electronic with Te, it is more electro-negative than Te. The incorporation of Se atoms in the Sb_2Te_3 lattice will change its lattice dynamics. The inset in fig. 2 summarizes the observed Raman shifts of different vibrational modes with the Se content and reveals that all the observed Raman active modes have a very small shift with the Se doping. Since the atomic masses of Sb and Te are comparable, the observed slight variation in A^1_{1g}, E^2_g and A^2_{1g} modes with the Se(x) content is anticipated for $Sb_2Te_{3-x}Se_x$ ($0.0 \le x \le 1.0$) mixed crystals, where the Se concentration is not significantly higher. However, a close observation of fig. 2 (inset) divulges that, initially, for low Se content ($x = 0.2$), the phonon frequencies shift to the lower wave number side. But with a further increase of Se, *i.e.*, for $x = 0.6$ and 1.0, the observed phonon frequencies gradually shift to the higher wave number side. The unit cell of Sb_2Te_3-like compounds has five quintuple layers (Te^1-Sb-Te^2-Sb-Te^1) weakly bound by the van der Waals force in which Te atoms exhibit two different environments, *i.e.*, Te^1 and Te^2. Te^2 atoms are the centre of mass of the lattice vibration [12] and the Raman active modes directly manifest the vibrational properties of the Sb-Te(2)/Te(1) bonds. The Sb-Te^2 bond is more polar than the Sb-Te^1 bond. Initially for a low concentration ($x = 0.2$), Se preferentially replaces Te at the Te^2 site, and, subsequently, for a higher concentration ($x = 0.6$, 1.0) the Se atoms continue to replace Te at Te^1/Te^2 sites in a random manner [21]. This might lead to the observed anomaly in phonon frequency

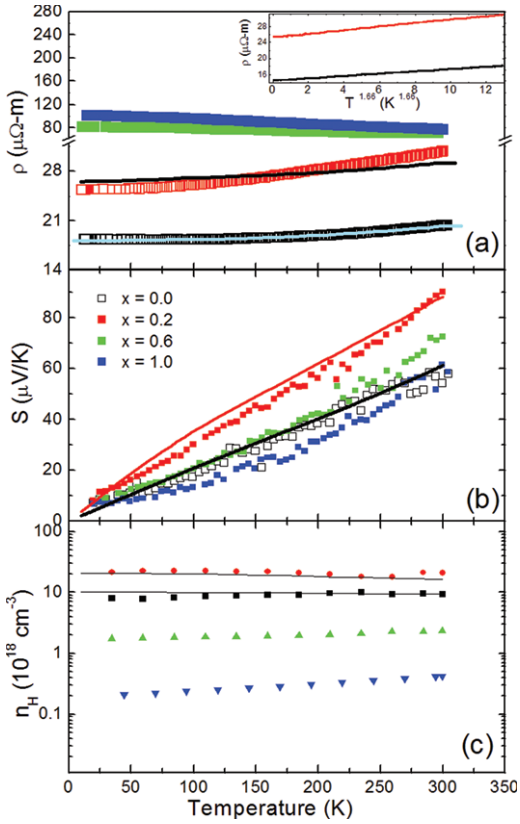

Fig. 3: (Color online) Experimental (points) and simulated (solid lines) temperature dependences of (a) the electrical resistivity ρ, (b) the Seebeck coefficient S, and (c) the Hall carrier concentration n_H for the $Sb_2Te_{3-x}Se_x$ ($x = 0.0$, 0.2, 0.6, and 1.0) samples. The simulation was performed simultaneously (with the same parameters) in the frame of the Boltzmann equation approach for the samples with the $x = 0.0$ and 0.2 Se content. The inset in (a) demonstrates the power-law fit, $\rho = \rho_0 + AT^n$ with $n \sim 1.66$ to the $\rho(T)$ data for the Sb_2Te_3 and $Sb_2Te_{2.8}Se_{0.2}$ samples.

for the $Sb_2Te_{2.8}Se_{0.2}$ sample (inset in fig. 2, marked with an arrow).

The $\rho(T)$ data of the polycrystalline $Sb_2Te_{3-x}Se_x$ samples depict that ρ increases with increasing Se concentration (fig. 3(a)). Pristine Sb_2Te_3 always possesses over-stoichiometric Sb atoms along with native point defects, *viz.*, V_{Te} and segregated Te [6,22,23]. The over-stoichiometric Sb atoms occupy prevailingly the Te^2 sites in the Te sublattice, giving rise to antisite (AS) defects of Sb_{Te} type. Due to such AS defects, Sb_2Te_3 always shows a p-type conductivity with hole concentration around $10^{20}\,\text{cm}^{-3}$ [9]. With increasing Se concentration, the formation energy of these AS defects increases. As a consequence the formation probability of AS defects decreases, which, in turn, leads to the decrease of the carrier (hole) concentration in $Sb_2Te_{3-x}Se_x$ samples with increasing x. Thus, ρ increases with increasing Se content for the reported $Sb_2Te_{3-x}Se_x$ alloys.

Figure 3(a) further depicts that while Sb_2Te_3 and $Sb_2Te_{2.8}Se_{0.2}$ samples exhibit weakly metallic ρ, but an

activated $\rho(T)$ behaviour is observed for higher-Se-content samples. The observed metallic $\rho(T)$ data, arising due to the increase of the intrinsic carrier concentration at high temperatures, are typical for these heavily doped narrow band semiconductors [24]. In order to extract the nature of carrier scattering in $Sb_2Te_{3-x}Se_x$ ($x = 0.0$, 0.2) samples, the $\rho(T)$ curve is fitted with the power-law expression $\rho = \rho_0 + AT^n$. For both the samples, the obtained best-fit value of n is 1.66. Recently Dutta *et al.* reported the same n value for Sb_2Te_3 crystals [8]. On the other hand, a similar value of n (= 1.3) for the $Sb_2Te_{3-x}Se_x$ system was also reported earlier by Kulbachiniskii *et al.* [5]. For bulk Sb_2Te_3 and the related TI systems, the transport properties of the surface state are often mixed with the bulk state, which probably gives rise to the unusual value of the exponent in the low-Se-content $Sb_2Te_{3-x}Se_x$ samples [6,8].

The $S(T)$ data depict that all the reported samples are of p-type in nature (fig. 3(b)). $S(T)$ initially increases with increasing x from $x = 0.0$ to 0.2. But for $x \geq 0.2$, $S(T)$ decreases. The compositional dependence of the scattering parameter (r) is estimated from the $S(T)$ data. For a heavily doped semiconductor (for a single valley in the isotropic case), S is given by [13]

$$S = \pm\frac{k_B}{e}\left[\eta_F - \frac{(r+5/2)F_{r+3/2}(\eta_F)}{(r+3/2)F_{r+1/2}(\eta_F)}\right]. \quad (1)$$

Here $\eta_F = E_F/(k_BT)$ is the reduced Fermi energy; the parameter r describes the energy dependence of the scattering time, and

$$F_n = \int_0^\infty d\eta \frac{\eta^n}{1+\exp(n-n_F)} \quad (2)$$

is the Fermi integral. Now, $r = -0.5$ corresponds to the acoustic phonon scattering, $r = 0.5$ is the scattering due to optical phonons and $r = 1.5$ denotes the scattering by ionized impurities. We estimate the Fermi energy (E_F) in two samples, *viz.*, Sb_2Te_3 and $Sb_2Te_{2.8}Se_{0.2}$, exhibiting metallic behaviour by a simple model,

$$E_F = \frac{\hbar^2}{2m^*}\left[3\pi^2 n_H\right]^{2/3}, \quad (3)$$

where n_H is the carrier concentration (fig. 3(c)). Reasonable values of $E_F \approx 100$ meV and 120 meV are obtained, respectively, for $x = 0.0$ and 0.2 samples [25,26]. Using these Fermi energies and formulae (1) and (2) we may estimate the scattering parameter r. Such procedure yields $r = -0.5$ and $r = 0.1$, respectively for $x = 0.0$ and $x = 0.2$ alloys. The obtained best-fit value of $r = -0.5$ for Sb_2Te_3 alloy (*i.e.*, $x = 0.0$) corroborates the reported results [13]. The $S(T)$ data thus reveal that in SbTeSe-based degenerated semiconductors, the increase of the Se content shifts the scattering from the preferentially acoustic phonon closer to impurity scattering.

For the $Sb_2Te_{2.4}Se_{0.6}$ and Sb_2Te_2Se samples, the activation energy (E_{act}) is estimated from the $\rho(T)$ data using the relation

$$\rho = \rho_0 \exp\left(\frac{E_{act}}{2k_BT}\right), \quad (4)$$

where ρ_0 is a constant. The estimated E_{act} values, 9.24 meV and 12.30 meV respectively for $Sb_2Te_{2.4}Se_{0.6}$ and Sb_2Te_2Se, indicate that the estimated transport gap (E_{act}) is much smaller than the reported band gap (E_g) [27]. E_g arises due to the difference between the lower conduction band (LCB) and the upper valence band (UVB) [22]. However, according to Akrap *et al.*, while E_g is determined by the band structure, E_{act} is actually linked to the presence of point defects [13]. Sb_2Te_3 hosts various kinds of defects, *viz.*, AS defects of Sb_{Te} type, V_{Te} and segregated Te. Increasing the Se content in the Sb_2Te_3 matrix enhances the interplay between these defects with Se atoms initially replace Te^2 atoms, but for a higher concentration it continues to replace Te^1/Te^2 atoms randomly. This might lead to the observed change from a metallic to an activated behaviour in the $\rho(T)$ data for $x > 0.2$. The energy state due to the native defects in the $Sb_2Te_{3-x}Se_x$ system probably lies between LCB and UVB and leads to a smaller E_{act} in the activated samples. Further, when the composition is tuned from Sb_2Te_3 to Sb_2Te_2Se, the concentration of holes in the system decreases. Around the composition $x = 1$ (Sb_2Te_2Se), the Se/Te sublattice is expected to be ordered with an almost complete compensation of donor and acceptor impurities [13]. Therefore, around $x = 1$ the bulk conductivity should be minimum, which is correctly reflected in our $\rho(T)$ data (see fig. 3(a)).

Figure 3(c) represents the thermal variation of n_H data for all the $Sb_2Te_{3-x}Se_x$ samples, measured in a magnetic field of 12 T. Like the $S(T)$ data initially with increasing x, n_H increases for Sb_2Te_3 and $Sb_2Te_{2.8}Se_{0.2}$, but for $x \geq 0.2$, it decreases, indicating that the apparent hole concentration is highest in $Sb_2Te_{2.8}Se_{0.2}$. Here we would like to present a plausible explanation for such anomalous behaviour of n_H in $Sb_2Te_{3-x}Se_x$. The band structure calculation indicates that the UVB of Sb_2Te_3 consists of six ellipsoids and the lower valence band (LVB) is known to be multivalleyed [5,24]. While explaining the Shubnikov-de Haas (SdH) and transient thermoelectric effect (TTE) data for the $Sb_2Te_{3-x}Se_x$ ($0.0 \leq x \leq 1.0$) system Kulbachinskii *et al.* indicate the presence of another valence band (NVB) for $x \geq 0.2$ and clearly predict two different regions, *viz.*, $0 \leq x \leq 0.2$ and $0.2 < x \leq 1.0$ in the band structure [5]. In the first region $0 \leq x \leq 0.2$, only UVB and LVB contribute. But in the second region $0.2 < x \leq 1.0$ the contribution comes from UVB, LVB and NVB, where NVB moves up and UVB moves down due to Se doping. It should be mentioned that UVB and LVB are not equally populated, the ratio of the density of holes in LVB to that of UVB is around 390 [28]. In view of this large ratio, LVB contributes mostly in the conduction mechanism. The evaluation of the band structure with the Se content in the $Sb_2Te_{3-x}Se_x$ ($0.0 \leq x \leq 1.0$) alloy as predicted by Kulbachinskii *et al.* [5], and correspondingly

Table 2: The simulated parameters of the investigated Sb_2Te_3 and $Sb_2Te_{2.8}Se_{0.2}$ alloys obtained by fitting the experimental temperature dependences of the Seebeck coefficient, the resistivity, and the Hall carrier concentration.

			Sb_2Te_3 $[R\bar{3}m]$	$Sb_2Te_{2.8}Se_{0.2}$ $[R\bar{3}m]$
Bandgap (eV)			0.25	0.25
Second valance band (eV)			0.19	0.08
Effective masses (m_0)	Light Holes		0.043	0.043
	Heavy Holes		0.15	0.15
		b1	0.705	0.705
	Light Holes	b2	0.615	0.615
Band extrema positions (b)		b3	0.615	0.615
		b1	0.534	0.534
	Heavy Holes	b2	0.341	0.341
		b3	0.341	0.341
Acceptor concentration (cm^{-3})			2.0×10^{19}	2.3×10^{19}
Scattering parameters	Density (kg/m^3)		6500	6500
	Sound velocity (m/s)		1780	1780
	Deformation potential (eV)		3	3
Grain boundaries	Grain size (nm)		15.3	10
	Scattering constant		0.3	0.3
Dielectric constant			101	101

the net contribution of the carrier from UVB, LVB and NVB might be related to the experimentally observed n_H behaviour.

In the framework of the Boltzmann equation approach, we simulated simultaneously (with the same parameters) $\rho(T)$ (see fig. 3(a)), $S(T)$ (see fig. 3(b)), and $n_H(T)$ (see fig. 3(c)) for the samples with $x = 0.0$ and 0.2. Theoretical dependences are shown in fig. 3(a)–(c) by solid lines. However, we were unable to reproduce a small value of the Seebeck coefficient in samples with $x = 0.6$ and $x = 1.0$ Se content without an unrealistic change of the band parameters. We suggest that part of holes in the material is localized and to fit data for samples with high Se content the localization of part of the holes should be taken into account. The theoretical model and the method of calculation are described in ref. [5]. In the fitting following scattering mechanisms were taken into account: acoustic phonon scattering, ionized acceptors scattering, grain boundary scattering. All acceptors were assumed to be ionized. Other parameters, *viz.*, effective masses, band edges, deformation potential, acceptor concentration, etc., are taken from the literature. For the fitting of the sample with $x = 0.2$ Se content, only the position of the second valence band, grain size and acceptor concentration were changed with respect to Sb_2Te_3. The details of the simulated parameters are provided in table 2. The optimal fitting value for the distance between valence bands is larger than the one that was experimentally obtained earlier [28]. This is probably due to the localization of the part of the holes in the investigated samples. This could be also origin of the very small Seebeck coefficient in the samples with $x = 0.6$ and $x = 1.0$. For these samples ($x = 0.6$, 1.0) the localization of the part of the holes can explain the

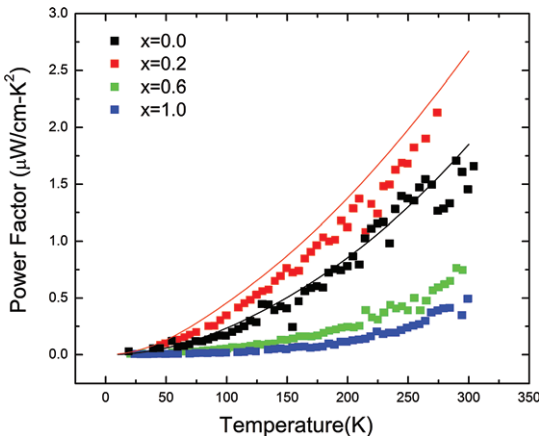

Fig. 4: (Color online) Thermal variation of thermoelectric power factor for the $Sb_2Te_{3-x}Se_x$ ($x = 0.0$, 0.2, 0.6, and 1.0) samples. Points denote experimental data and solid lines represent the theoretical fit.

$\rho(T)$ data, which has an activated character (see fig. 3(a)). These samples have too large value of the Hall coefficient and a small value of the Seebeck coefficient. One of the reasons may be (probably) due to modification of the band structure with high Se content [5] and localization of the part of the holes.

Figure 4 shows the compositional dependence of PF for the $Sb_2Te_{3-x}Se_x$ samples estimated from the measured quantities. The theoretical values of PF for the Sb_2Te_3 and $Sb_2Te_{2.8}Se_{0.2}$ alloys, calculated from the simulated $S(T)$ and $\rho(T)$ data, are also plotted in fig. 4. The PF increases with increasing temperature and reveals a non-saturating behaviour around room temperature. Similar to the behaviour observed for the $S(T)$ and $n_H(T)$

data, the maximum value of PF is also observed for the $Sb_2Te_{2.8}Se_{0.2}$ alloy. This further indicates that increasing the Se content in Sb_2Te_3 does not always contribute a positive role in increasing the thermoelectric performances of $Sb_2Te_{3-x}Se_x$ samples. However, conclusive evidence can be drawn only after estimating ZT. It should be recalled that $Sb_2Te_{2.8}Se_{0.2}$ possess the highest n_H ($\sim 10^{19}$/cc). It is thus quite justified to assume that tuning of the carrier concentration as well as band structure engineering including the optimization of the band parameters in the $Sb_2Te_{3-x}Se_x$ system should play a crucial role in obtaining a good TE material.

Conclusion. – XRD data and Raman spectra confirm that all the synthesized $Sb_2Te_{3-x}Se_x$ samples exhibit rhombohedral crystal geometry. It has been realized that the surface states are often mixed with the bulk state, giving rise to the observed metallicity in the Sb_2Te_3 and $Sb_2Te_{2.8}Se_{0.2}$ samples. The transport gap (E_{act}), estimated in high-Se-content samples showing an activated behavior, is smaller than the reported band gap (E_g) probably due to the presence of point defects and of the tail of the density of state. Acoustic phonon scattering dominates the $S(T)$ data for the synthesized host Sb_2Te_3. However, with increasing Se concentration, impurity scattering gradually dominates the $S(T)$ data. The theoretical calculation, based on a four-band model, demonstrates that the position of the second valance band as well as the acceptor concentration are sensitive to the Se concentration and to the part of the holes in high-Se-content samples is localized.

* * *

The work is supported by DST, Government of India-RFBR, Government of Russia (DST reference No.: INT/RUS/RFBR/P-183; RFBR grant: IND-a 15-52-45037). The financial grant, including the fellowship of the first author DD, received from the UGC-DAE Consortium for Scientific Research, Kalpakkam node (Project reference No.: CSR-KN/CRS-65/2014-15/505) is also gratefully acknowledged. The authors would also like to thank the DST, Government of India, for low-temperature high-magnetic-field facilities at UGC-DAE CSR, Kolkata Centre.

REFERENCES

[1] Nolas G. S., Sharp J. and Goldsmid H. J., *Thermoelectrics: Basic Principles and New Materials Developments* (Springer, New York) 2001.
[2] Behnia K., *Fundamentals of Thermoelectricity* (Oxford University Press, UK) 2015.
[3] Dresselhaus M. S., Chen G., Tang M. Y., Yang R., Lee H., Wang D., Ren Z., Fleurial J. P. and Gogna P., *Adv. Mater.*, **19** (2007) 1043.
[4] Fan S., Zhao J., Guo J., Yan Q., Ma J. and Hng H. H., *Appl. Phys. Lett.*, **96** (2010) 182104.
[5] Kulbachinskii V. A., Dashevskii Z. M., Inoue M., Sasaki M., Negishi H., Gao W. S., Lostak P., Horak J. and Visser A. D., *Phys. Rev. B*, **52** (1995) 10915.
[6] Das D., Malik K., Deb A. K., Dhara S., Bandyopadhyay S. and Banerjee A., *J. Appl. Phys.*, **118** (2015) 045102.
[7] Da Silva L. W., Kaviany M. and Uher C., *J. Appl. Phys.*, **97** (2005) 114903.
[8] Dutta P., Bhoi D., Midya A., Khan N., Mandal P., Sanatham S. S. and Ganesan V., *Appl. Phys. Lett.*, **100** (2012) 251912.
[9] Horak J., Karamazov S., Nesladek P. and Lostak P., *J. Solid State Chem.*, **129** (1997) 92.
[10] Lostak P., Novotny R. and Bene L., *J. Cryst. Growth*, **94** (1989) 656.
[11] El-Sayad E. A. and Sakr G. B., *Cryst. Res. Technol.*, **40** (2005) 1139.
[12] Soni A., Yanyuan Z., Ligen Y., Aik M. K. K., Dresselhaus M. S. and Xiong Q., *Nano Lett.*, **12** (2012) 1203.
[13] Akrap A., Ubaldini A., Giannini E. and Forro L., *EPL*, **107** (2014) 57008.
[14] Malik K., Das D., Mondal D., Chattopadhyay D., Deb A. K., Bandyopadhyay S. and Banerjee A., *J. Appl. Phys.*, **112** (2012) 083706.
[15] Vanberkum J. G. M., Sprong G. J. M., Keijser T. D., Delhez R. and Sonneveld E. J., *Powder Diffr.*, **10** (1995) 129.
[16] Lutterotti L., Matthies S. and Wenk H. R., in *Proceeding of ICOTOM14*, edited by Spunar J. A. (National Research Council of Canada, Ottawa) 1999, p. 1599; *IUCr CPD Newsletter*, No. 21 (1995) p. 14.
[17] Basu R., Bhattacharya S., Bhatt R., Sing A., Aswal D. K. and Gupta S. K., *J. Electron. Mater.*, **42** (2013) 2292.
[18] Shahil K. M. F., Hossain M. Z., Goyal V. and Balandin A. A., *J. Appl. Phys.*, **111** (2012) 054305.
[19] Kim Y., Chen X., Wang Z., Shi J., Miotkowski I., Chen Y. P., Sharma P. A., Lima Sharma A. L., Hekmaty M. A., Jiang Z. and Smirnov D., *Appl. Phys. Lett.*, **100** (2012) 071907.
[20] Sosso G. C., Caravati S. and Bernasconi M., *J. Phys.: Condens. Matter*, **21** (2009) 095410.
[21] Drabble J. R. and Goodman C. H. L., *J. Phys. Chem. Solids*, **5** (1958) 142.
[22] Abrikosov N. K., Poretskaya L. V. and Ivanova I. P., *Zh. Neorg. Khim.*, **4** (1959) 2525.
[23] Karamazov S., Nesladek P., Horak J. and Matyas M., *Phys. Status Solidi (b)*, **194** (1996) 187.
[24] Blank V. D., Buga S. G., Kulbachinskii V. A., Kytin V. G., Medvedev V. V., Popov M. Y., Stepanov P. and Skok V. F., *Phys. Rev. B*, **86** (2012) 075426.
[25] Kulbachinskii V. A., Kaminsky A. Y. and Lunin R. A., *Semicond. Sci. Technol.*, **17** (2002) 1133.
[26] Kulbachinskii V. A., Kytin V. G., Kudryashov A. A. and Tarasov P. M., *J. Solid State Chem.*, **193** (2012) 47.
[27] Skinner B., Chen T. and Shklovskii B. I., *Phys. Rev. Lett.*, **109** (2012) 176801.
[28] Kulbachinskii V. A., Miura N., Nakagawa H., Drashar C. and Lostak P., *J. Phys.: Condens. Matter*, **11** (1999) 5273.